Formability Analysis of Diode-Laser-Welded Tailored Blanks of Advanced High-Strength Steel Sheets

S.K. PANDA, V.H. BALTAZAR HERNANDEZ, M.L. KUNTZ, and Y. ZHOU

Currently, advances due to tailored blanking can be enhanced by the development of new grades of advanced high-strength steels (HSSs), for the further weight reduction and structural improvement of automotive components. In the present work, diode laser welds of three different grades of advanced high-strength dual-phase (DP) steel sheets (with tensile strengths of 980, 800, and 450 MPa) to high-strength low-alloy (HSLA) material were fabricated by applying the proper welding parameters. Formability in terms of Hecker's limiting dome height (LDH), the strain distribution on the hemispherical dome surface, the weld line movement during deformation, and the load-bearing capacity during the stretch forming of these different laser-welded blanks were compared. Finite element (FE) analysis of the LDH tests of both the parent metals and laser-welded blanks was done using the commercially available software package LS-DYNA (Livermore Software Technology Corporation, Livermore, CA); the results compared well with the experimental data. It was also found that the LDH was not affected by the soft zone or weld zone properties; it decreased, however, with an increase in a nondimensional parameter, the "strength ratio" (SR). The weld line movement during stretch forming is an indication of nonuniform deformation resulting in a decrease in the LDH. In all the dissimilar weldments, fracture took place on the HSLA side, but the fracture location shifted to near the weld line (at the pole) in tailor-welded blanks (TWBs) of a higher strength ratio.

I. INTRODUCTION

A. Advanced High-Strength Steel Sheets

Recently, there has been significant improvement in the versatility of formable steel grades for automotive stampings. Automotive steels can generally be categorized into three classes: lower-strength steels (mild, interstitial-free, and extra-deep drawing-quality steels); high-strength steels (HSSs) (high-strength low-alloy (HSLA), carbon-manganese, bake-hardening, and high-strength interstitial-free steels); and advanced HSSs (AHSSs) (dual-phase (DP), transformation-induced plasticity, complex-phase, and martensitic steels). The principal differences between HSSs and AHSSs are related to their microstructure and strengthening mechanisms. The HSS steels, which are mainly ferritic, are strengthened by grain refinement and by precipitation hardening, which is achieved by microalloying additions. The AHSSs are multiphase steels that are manufactured with an intercritical annealing step designed to produce a ferrite and austenite bimodal microstructure, which, upon cooling, results in a ferritic matrix with dispersed decomposition products such as martensite and bainite and, in some cases, retained austenite. The AHSSs exhibit yield strengths (YSs) similar to the HSSs; however, during deformation, they exhibit persistent strain hardening, which results in higher ultimate strengths with good ductility.[1] Thus, AHSSs have superior combinations of strength and formability, while being reasonably simple and inexpensive to manufacture. These characteristics are desirable for weight reduction, structural improvement, and reduction in the costs of structural automotive components.

B. Tailored-Welded Blanks and Challenges

Tailor-welded blanks (TWBs) are fabricated by welding multiple sheets of different shapes, grades, and thicknesses together in a single plane, after which the weldment is then stamped into a three-dimensional shape.[2,3] The concept of combining different steel grades into a single welded blank enables manufacturing engineers to "tailor" the blank such that various steel properties are optimized within the part. For example, TWBs give the designer the flexibility to eliminate reinforcements while improving the structural and dimensional characteristics by putting a higher-strength material at high-stress locations.[4]

The forming behavior of a TWB, however, will be influenced by many factors, such as: material property changes in the fusion zone (FZ) and heat-affected zone (HAZ) of the weld;[5–9] the effects of the weld on the strain distribution, failure site, and crack propagation;[4,8,10] and nonuniform deformation due to the differences in thickness,[4,8,11] properties, or surface

S.K. PANDA, Postdoctoral Fellow, Department of Mechanical Engineering, and V.H. BALTAZAR HERNANDEZ, Doctoral Student, M.L. KUNTZ, Research Professor, and Y. ZHOU, Professor, Centre for Advanced Materials Joining, are with the University of Waterloo, Waterloo, ON, Canada. Contact e-mail: s2panda@engmail.uwaterloo.ca; panda_sushanta@yahoo.co.in
Manuscript submitted November 14, 2008.
Article published online June 16, 2009.

characteristics.[8] Because of these additional complexities, some important factors that influence the potential formability of the TWBs are the thickness ratio;[11] the difference in sheet properties, weld, and HAZ properties;[7,9] and the weld orientation with respect to the major strain,[10] weld position,[12] and draw bead design.[13]

Several past studies have concentrated on the deep drawing and stretch forming of TWBs composed of similar materials and different thicknesses. Very few studies have been reported on the formability of tailored blanks of dissimilar combinations in stretch forming.[14,15] No open research literature has been found on the formability of dissimilar tailored blank combinations of AHSSs (different DP steels) with HSLA during stretch forming.

Shao *et al.*[16] studied the formability of TWBs composed of dissimilar combinations of different HSSs with mild steel sheets. They conducted the equiaxial stretch-forming test using a 25.4-mm hemispherical punch (Erichsen cup test). The Erichsen and Olsen tests were developed to estimate the sheet metal formability under pure stretching conditions; however, neither of these simulative tests gives a reliable overall formability index for a stamping operation. The major problems associated with these tests are the insufficient penetrator size, the inability to prevent the drawing-in of the flange, and the poor correlation of the tests with press performance. It is difficult to achieve good reproducibility with these tests, even with the same experimental setup.[17,18] Hecker[17] developed a modified hemispherical cup test by scaling the penetrator size up to 101.6 mm and adding a draw bead in the die plates near the die opening, to prevent draw-in. This experimental test is known as the limiting dome height (LDH) test. The reproducibility of the results is improved with the LDH test; in addition, the correlation between the cup height and the *n* value for low-carbon steels is good.

C. *Objectives*

The TWBs are particularly attractive when combined with an AHSS for potential engineering solutions to further weight reduction and cost reduction with improved part performance. Hence, it is important to understand the formability of TWBs made with different AHSS sheets. Therefore, in this work, three different grades of DP steels (DP980, DP800, and DP450) were laser welded with an HSLA steel, to produce three

combinations of TWBs. The formability in terms of the LDH for these composite blanks was studied in comparison with the monolithic parent metals. The strain distribution, weld line movement, failure location, and load-bearing capacity during stretch forming were also analyzed, to select the optimum combinations. Finite element (FE) analysis of the LDH testing was done and the predicted results were compared to the experimental data.

II. MATERIAL SELECTION AND PROPERTIES

Three grades of DP steels (DP980, DP800, and DP450) and one grade of HSLA steel were selected for the formability analysis. Because the full chemical composition of the steel sheets was considered proprietary, a summary of the thickness, hardness, and major alloying elements is provided in Table I, including the carbon equivalent (CE), using the well-known Yurioka formula.[19] The mechanical properties for these materials, such as the yield strength (YS), ultimate tensile strength (UTS), strength coefficient (K), strain-hardening exponent (*n*), percent elongation (total and uniform), and Lankford's anisotropy parameters, are shown in Table II. The K and *n* values of these steels were evaluated by fitting the experimental true stress and true strain values with the analytical Hollomon's power law of hardening, as discussed previously.[8] There were significant differences in the mechanical properties of the grades. The ratio of the UTS to the YS was higher in the DP steels than in the HSLA. This was due to the higher UTS of the DP steels as compared to the HSLA steels. Microstructural examination showed that the DP steels consisted of a ferrite matrix with dispersed islands of martensite. The DP steels are strengthened by the interaction of the different phases and the strain transfer from the soft ductile ferrite phase to the harder martensite phase.[20] The strain-hardening rate during plastic deformation in these multiphase steels depends on the volume fraction, size, morphology and distribution of the hard phase.[20]

The DP450, with 7 pct volume fraction martensite (f_M), had a higher uniform elongation and *n* value compared to the DP980 and DP800 steels (both with approximately 50 pct f_M). Figure 1 shows the engineering stress–engineering strain diagrams for the HSLA and DP450. A distinct yield region was observed in the HSLA, with the formation of Luder bands during

Table I. Different Steel Sheets Used in Present Study

| Grade | Thickness (mm) | Chemical Composition (Weight Percent) | | | | | | | $f_M^\dagger$ (Pct) | Hardness (HV) |
		C	Mn	Mo	Si	Cr	Al	CE*		
HSLA	1.14	0.080	0.827	0.007	0.454	0.034	0.048	0.182	—	175 ± 4
DP450	1.20	0.071	1.431	0.013	0.042	0.489	0.040	0.266	7	157 ± 4
DP800	1.25	0.147	1.719	0.018	0.294	0.612	0.036	0.525	54	278 ± 3
DP980	1.17	0.135	2.100	0.350	0.050	0.150	0.450	0.540	49.4	273 ± 4

*CE $= C + A(C)\left(\frac{Mn}{6} + \frac{Si}{24} + \frac{Cr+Mo+V}{5} + \frac{Cu}{15} + \frac{Ni}{20} + \frac{Nb}{5} + 5B\right)$ and $A(C) = 0.75 + 0.25\tanh[20(C - 0.12)]$.
†The term f_M represents the volume fraction of martensite.

Table II. Mechanical Properties of Steel Sheets

Steel Grade	YS (MPa)	UTS (MPa)	K (MPa)	n	Total Elongation (Pct)	Uniform Elongation (Pct)	Lankford Parameters			
							R_0	R_{45}	R_{90}	$\bar{R}^*$
HSLA	413	463	756.8	0.18	32.97	14.23	0.75	1.26	1.11	1.10
DP450	298	491	835.1	0.20	31.43	20.01	1.03	0.87	1.51	1.07
DP800	544	885	1404.1	0.15	18.71	12.16	0.87	1.13	0.91	1.01
DP980	534	980	1510.0	0.14	15.20	11.57	0.80	0.93	0.85	0.88

$^*\bar{R} = \frac{R_0 + 2R_{45} + R_{90}}{4}$.
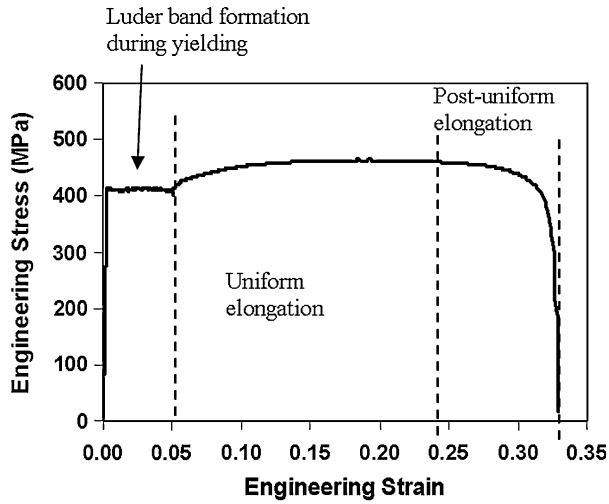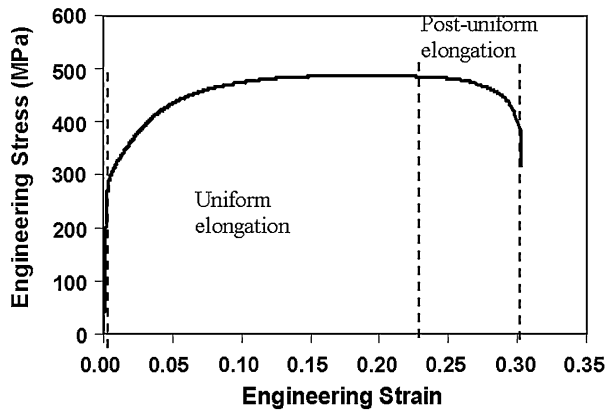
Fig. 1—Uniform elongation regions in engineering stress–engineering strain for (a) HSLA and (b) DP450 steels.
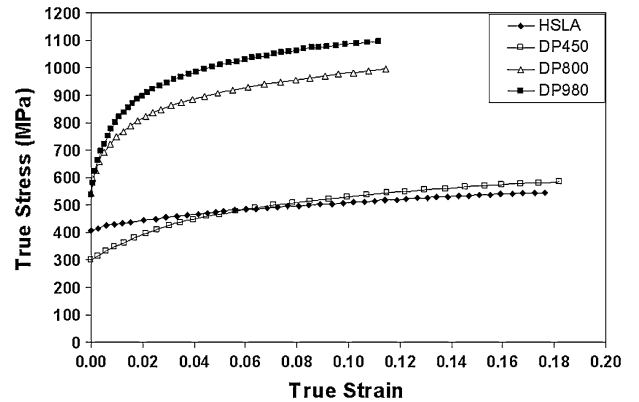

Fig. 2—True stress–true strain diagram of different steels sheets used in the present study.

were higher in the DP450. A comparison of the experimental true-stress-vs-true-strain curves for the four steels is shown in Figure 2.

III. EXPERIMENTAL PROCEDURE

A. Preparation of TWBs

The HSLA was welded in combination with each of the DP steels (DP450, DP800, and DP980). A 4-kW AlGaAs diode laser* with a wavelength of 805 ± 5 nm

*4-kW AlGaAs diode laser is a registered trademark of Coherent Inc., Santa Clara, CA.

was used to prepare the blanks. The beam was rectangular in shape, with minimum dimensions of 12×0.9 mm. The beam had a focal length of 80 mm and was focused on the top surface of the sheet. Due to the relatively low power density of the diode laser, the welds were produced in the conduction mode. Thus, in order to achieve full penetration, the welding speeds were limited to between 1.0 and 1.2 m/min. The TWBs were fabricated with the weld line oriented transverse to the rolling direction. The sheets were aligned and clamped so that there was no mismatch or gap between the edges. Before each weld, the laser beam was aligned with the joint, to ensure an equal and consistent amount of melting in both sheets.

tensile testing; in the DP450 steel, however, there was a continuous transition from elastic to plastic deformation. Similar transitions were also observed in the DP800 and DP980 steels; it was difficult, therefore, to define an exact yield point. Thus, the 0.2 pct proof stress, as determined from the stress-strain curve, was taken for the YS of the DP steels. The total elongation was higher in the HSLA steel as compared to the DP450; however, the uniform elongation and the n value

B. *Metallography and Microhardness Testing*

Through-thickness cross sections were cut from representative laser-welded specimens and were mounted and polished as per standard metallographic procedures. The polished specimens were etched with a 2 pct Nital solution; the microstructure was observed using optical and scanning electron microscopy (SEM) across the welded region, from one side of the parent metal to the other. The weld profile was observed, to check for penetration and to identify the welded regions. Cross-weld hardness profiles were obtained using a straight line of microhardness indentations with a 0.5-mm spacing under a load of 500 g for 10 seconds.

C. *Stretch-Forming Experiments*

The Hecker's LDH tests[17] were performed using a 101.6-mm-diameter hemispherical punch on a hydraulic press (MTS 866, Metal Form Press**). A schematic

diagram of the arrangement of tools (punch, lower die, and upper die) used in the experiments can be found in Reference 5. Square specimens 190 × 190 mm in size were cut from the laser-welded blanks. To measure the major and minor strains after deformation, the blanks were marked with a grid of circles (2.5 mm in diameter) using electrochemical etching. The laser-welded blanks were placed on the lower die such that the weld line was at the middle of the die opening with the welded side facing up. The blanks were clamped by a draw bead provided in the dies. The experiment was conducted at a punch speed of 2 mm/min; the test was stopped when a visible neck or initiation of fracture was observed on the specimen. Care was taken to maintain a constant punch velocity; however, minor variations may have caused very small changes in the strain rate. These changes did not affect the flow behavior of the steels, however, because of their low sensitivity to changes in the flow stress-strain behavior at room temperature.[21] A clamping force was applied between the upper and lower dies to ensure no draw-in from the flange during the experiments. A data acquisition system was used to record the load-displacement data during all of the stretch-forming experiments. All the LDH tests were conducted by placing a polyurethane sheet 0.05 mm in thickness between the punch and the blank. The difference in thickness was negligible and, hence, the misalignment of the TWB was within ±0.06 mm (half the difference between the thicknesses of the welded sheets). However, to maintain consistency during testing, the blank was oriented such that weld root side was toward the punch side.

The dome height of the specimens was determined from the load-displacement diagram obtained with a data acquisition system. The deformed elliptical grid-marks on the LDH specimens were classified according to safe, necked, and failed zones. The major and minor

diameters of the ellipses were measured by a strain analyzer (Model 100 Grid Analyzer)† and processed

with software (version 5.21, FMTI Systems, Inc.) used to calculated the major and minor strains. The ellipse at the topmost position of the deformed sample was referred to as the pole. Variations of major and minor strains across the weld were measured, to plot the strain distribution profiles as a function of distance from the pole. The weld line movement was measured at approximately 11 points on the weld line of the deformed specimens, using a digital height gage with a resolution of 0.01 mm.

IV. FE SIMULATION

Numerical simulation of the laboratory-based Hecker's LDH test was carried out using the explicit FE code LS-DYNA. The FE model used in previous studies[22] was used to study the effect of the weld FZ properties, soft zone properties, and parent metal properties on the LDH, strain distribution, and weld line movement. Davies *et al.*[23] studied the forming limit diagram (FLD) of aluminum TWBs using the Marciniak-Kuczynski (M-K) method with the Hosford yield criteria. In the present work, however, the FLD was predicted by a postprocessor solver using an empirical equation (Eq. [1]) that was suggested by the North American Deep Drawing Research Group.[24] After the FLD_0 was calculated from Eq. [1], the right and left sides of the limiting curve were plotted by the postprocessor with an offset equal to the difference between the calculated FLD_0 and the FLD_0 of the Keeler–Brazier forming limit curve.[24]

If

$$t < 2.54\,\text{mm},\ FLD_0 = \frac{n}{0.21}(23.3 + 14.13t) \qquad [1]$$

where t is the sheet thickness in millimeters and n is the strain-hardening coefficient of the sheet.

This model predicts the forming limits of the AHSS and HSLA reasonably well, as suggested by Bleck *et al.*[25] and Panda *et al.*[22] All tooling surfaces were modeled using rigid, four-node shell elements. The blanks were modeled using four-node quadrilateral Belytschko–Tsay[26] shells. The die was fixed and both the punch and binder were allowed movement in the z direction (along the axis of the punch). A load corresponding to the binder force in each experiment was applied to the binder to clamp the blank. Penalty-function-based contact interfaces were used to enforce the intermittent contact and sliding boundary conditions between the sheet metal and the tooling elements. The coefficient of friction between the blank and tools was assumed to be 0.125, due to the application of the polyurethane sheet.[27] The Barlat-89 nonquadratic yield criteria,[28] which account for the in-plane and transverse anisotropy, were used in modeling the deformable

blank. This model incorporates the effect of both the normal and planar anisotropy in the polycrystalline sheet during deformation, as shown here:

$$\Phi = a|K_1 + K_2|^m + a|K_1 - K_2|^m + c|2K_2|^m = 2\sigma_Y^m \quad [2]$$

where Φ is the yield function, σ_Y is the yield stress, m is Barlat's yield exponent, and K_1 and K_2 are stress tensor invariants;

$$K_1 = \frac{\sigma_x + h\sigma_y}{2} \quad [3]$$

$$K_2 = \sqrt{\left(\frac{\sigma_x - h\sigma_y}{2}\right)^2 + p^2\tau_{xy}^2} \quad [4]$$

where σ_x, σ_y, and τ_{xy} are plane stress components in orthotropic axes and a, c, h, and p are anisotropic material constants obtained from Lankford's parameters, as given in previous work.[22,28] In the present case, to understand the effect of the FZ and the HAZ, the model was constructed with the incorporation of a central hardened region and an outer softened zone on the DP side. The FE model of TWBs was also constructed without the incorporation of both the hard and soft zones, as per the previous work,[8] and the simulated LDH results were compared with the LDH obtained from the FE simulation with the incorporation of weld zones. The flow stress-strain behavior of the FZ of the DP980-DP980 laser-welded steel sheets was obtained by a minitensile specimen. The experimental flow curve data were used to define the properties of the FZ. Laser-welded transverse tensile testing and FE modeling were carried out, to obtain the load displacement through iterative curve fitting.[7] The obtained soft zone properties were validated for different laser welding conditions (diode and YAG laser). It was found that, with the incorporation of these properties into the FE modeling, the strain distribution and formability (elongation) were predicted well during the uniaxial tensile testing of the welded blank.[7] It was subsequently validated for a biaxial stretch forming of laser-welded, similar DP980 steel sheets.[22] The assigned properties for different zones in a dissimilar DP980-HSLA blank were justified with microstructure and microhardness analysis, as described in Section V.

The calculated major and minor strain data points at each step of the deformation in the FE simulation were superimposed on the FLD curve. For the failure prediction of the TWBs, the thickness and n value of the weaker sheet were used. The cup height at the first appearance of failure/necking was used to determine the LDH.

V. RESULTS AND DISCUSSION

A. Microstructure and Microhardness Analysis

The cross-weld hardness profile for the HSLA-DP980 blank is shown in Figure 3(a), along with the corresponding overview of the weld cross section (Figure 3(b)). The weld region labels correspond to the
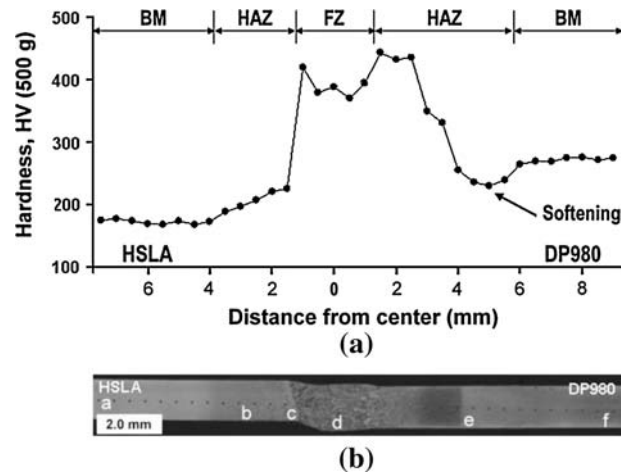

Fig. 3—(a) Hardness profile across the weld and (b) cross-sectional macrostructure for HSLA-DP980, showing respective hardness indentations.

microstructures, as observed under SEM, shown in Figure 4. The HSLA base metal (BM) microstructure was composed of a typical fine ferrite grain structure with a dispersion of carbides, as observed in Figure 4(a); the corresponding BM hardness was 175 ± 4 HV (Figure 3(a)). Figure 4(b) shows refined grains in the recrystallized zone at the edge of the HAZ. In Figure 4(c), grain coarsening was observed, with a predominantly sideplate microstructure in the HSLA HAZ near the fusion boundary. The FZ microstructure, as illustrated in Figure 4(d), was predominantly martensitic and also consisted of a mixture of ferrite allotriomorphs and bainite. The FZ hardness averaged 390 ± 10 HV. The same type of predominantly martensitic structure was found in the FZ of the DP980-DP980 laser-welded steel with an average hardness of 415.7 ± 7.7 HV in previous work.[5–7] Hence, the use of the same tensile flow properties for the FZ as were obtained from previous experiments is reasonable. The BM microstructure of the DP980, as depicted in Figure 4(f), consisted of a ferrite matrix with bands of martensite. The DP980 BM hardness measured 273 ± 4 HV. Tempering of the martensite phase was observed in the outer HAZ, as shown in Figure 4(e). Due to the tempering of martensite, the hardness was reduced by approximately 44 HV relative to the BM (Figure 3(a)). This phenomenon is termed "HAZ softening." The softened region extended (approximately 1.5 to 2 mm) from the edge of the intercritical HAZ toward the BM. The same degree of HAZ softening was also found during laser welding of the DP980 steel (i.e., in similar combination) in previous work.[5–7] It was also found that this softening was detrimental to the formability, due to strain localization in the soft zone during the LDH test.[22] Thus, the soft zone properties evaluated for the DP980-DP980 welds[7] were used in the case of the dissimilar DP980-HSLA combination

Figure 5 shows the corresponding cross-weld hardness profiles for the HSLA-DP800 and the HSLA-DP450 blanks. Measurable softening was observed in the outer HAZ of the DP800 steel. Softening was
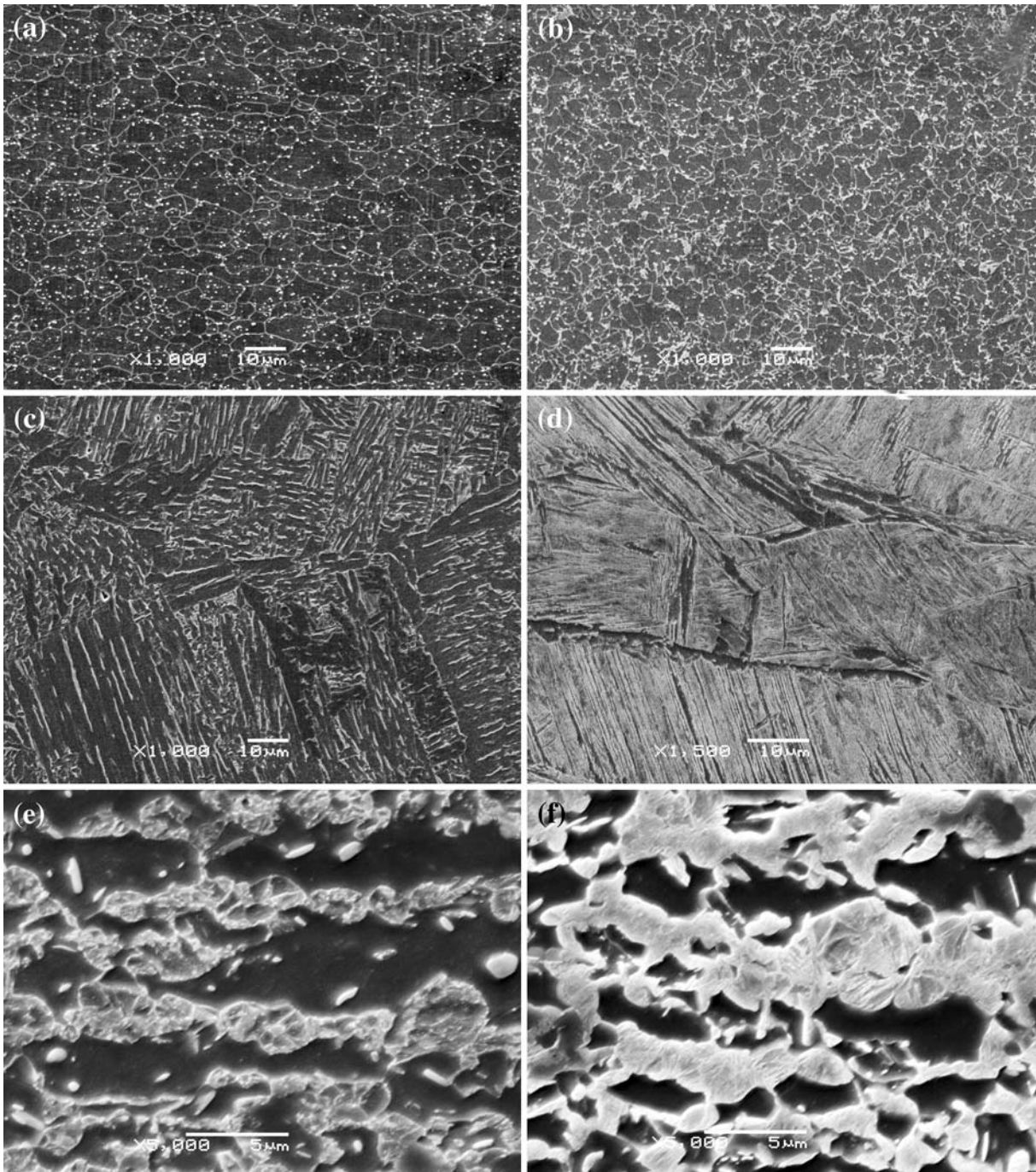
Fig. 4—SEM micrographs for dissimilar HSLA-DP980: (*a*) HSLA BM, (*b*) HSLA fine grain region, (*c*) HSLA coarse grain region, (*d*) FZ, (*e*) DP980 tempered martensite in the outer HAZ, and (*f*) DP980 BM.

immeasurable in the DP450, mainly due to the lower volume fraction of the BM martensite. Comparable results have been obtained for diode laser welding on various grades of DP steel.[29] The weld microstructure of HSLA-DP450 displayed a larger volume fraction of sideplate structures (not represented here); this was confirmed by the FZ hardness of 270 ± 4 HV (Figure 5). The relatively low CE of the DP450 compared to that of the DP800 and DP980 (Table I) resulted in the lowest FZ hardness when welded to the HSLA.

Differences in the FZ hardness in the dissimilar combinations were influenced by variations in the chemical composition through mixing. It was confirmed by experimental analysis of the FZ chemistry, which suggested dilution between the paired sheets and which was consistent with referenced work regarding the welding of dissimilar grades of AHSS.[30] During the stretch forming of a nonhomogeneous dissimilar laser-welded blank, fracture may be expected to initiate from three possible locations, *e.g.*, the weaker BM, the FZ, or
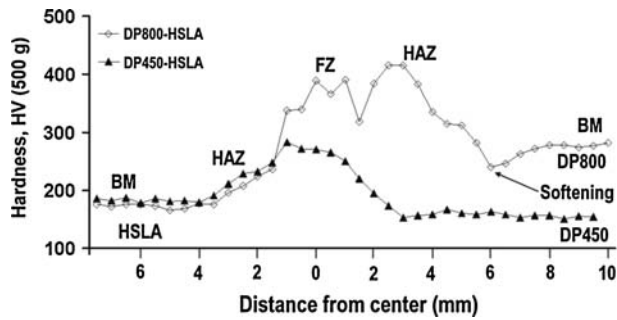
Fig. 5—Hardness profiles for HSLA-DP980 and HSLA-DP450 dissimilar combinations.
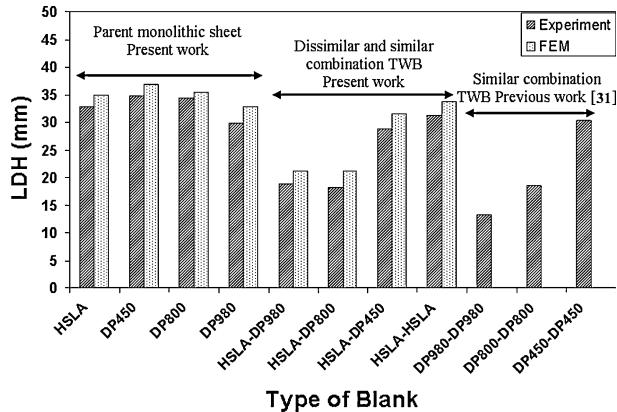

Fig. 6—Comparison of LDH of parent metals and TWBs of different combinations.

the soft zone. If fracture will initiate in the weldment (in either the FZ or the soft zone) during the forming of the dissimilar welded blank, then the influence of the weld zone should be accessed in order to understand the effect of the weld properties and the geometry. Otherwise, the difference in the material properties should be analyzed, which will shift the fracture location to the weaker HSLA side. Hence, the effect of the weld zone on formability and the need to evaluate its properties depends on the fracture locations during forming. The detailed analysis is presented in the remainder of this section.

B. LDH

The LDH measured at the point of necking/failure in the stretch forming of the parent metal monolithic blanks and the TWB combinations is shown in Figure 6. It was found that the DP450 and DP980 had the highest and lowest LDH, respectively, among the range of parent metals that were investigated. For the parent metals, the LDH depended on both the strain-hardening exponent (n value) and the thickness of the sheet (Eq. [1]). It is known that the LDH is higher for thicker sheets and higher n values. This is due to the increased deformation before thinning and the uniform strain distribution on the dome surface. Among the laser-welded blanks, the LDH was highest when the HSLA was welded to itself (i.e., HSLA-HSLA). The LDH of

the dissimilar-material laser-welded blanks decreased with the increasing BM strength of the paired steel, i.e., the HSLA-DP450 to HSLA-DP980. The stretch-formed hemispherical dome specimens are shown in Figure 7. There was 40 pct decrease in the LDH of the HSLA-DP980 and HSLA-DP800 laser-welded blanks as compared to the HSLA monolithic sheet. The LDH of the HSLA-DP800 was slightly lower than that of the HSLA-DP980, mainly due to the difference in thickness between the DP800 and DP980 parent sheets. The nominal sheet thickness was 1.2 mm; however, there were slight variations in the sheet thickness, as shown in Table I. Thus, the decrease in the LDH with the increasing BM strength in combination with the HSLA was affected by differences in both the strength and the thickness between the sheets.

In the LDH testing of the DP980-DP980 and DP800-DP800 laser-welded blanks, failure was found to invariably occur in the softened region of the HAZ. Hence, there is a significant decrease in the LDH in these laser-welded blanks as compared to the monolithic parent sheet. However, there is only a 12 pct decrease in the LDH for the DP450-DP450 laser-welded blank compared to the LDH of its parent monolithic sheet (DP450). This was due to the lower volume fraction of martensite in DP450; hence, there was no significant softening observed in the outer HAZ as compared to DP980 and DP800.[31] In the dissimilar combinations, there was no necking or fracture in the soft zone, as observed in the similar combination of laser-welded DP980 and DP800 blanks. This was due to the hardness and strength[7] of the softened HAZ in comparison with the HSLA BM. As shown in Figures 3 and 5, even though the HSLA side did not experience any softening, the BM was still softer than the HAZ of the DP steels; hence, necking/fracture occurred in the HSLA side.

The predicted LDH from the FE simulations corresponded well with the experimental values, as shown in Figure 6. The predicted LDH was consistently higher than the monolithic and welded blanks, because of simplifying assumptions such as the coefficient of friction between the tools and blank, the Barlat yield criteria, the stress-strain constitutive relation during deformation of the blank material, and the failure criteria. It was also found that incorporation of the weld properties or soft zone properties did not significantly change the predicted LDH (the FE-predicted LDH was 21.17 mm with the incorporation of the FZ and soft zone properties, 21.17 mm without the soft zone properties, and 21.2 mm without the incorporation of the complete weld zones in the modeling for the DP980-HSLA dissimilar laser-welded blank). This occurred for the following reasons.

(a) The incorporation of the softened zone properties during the FE simulation was not important, because the region was stronger than the HSLA side parent metal and, hence, there was no strain localization in the softened zone.
(b) Similarly, incorporation of the very narrow weld zone did not influence the FE results, because fracture does not propagate across the weld and
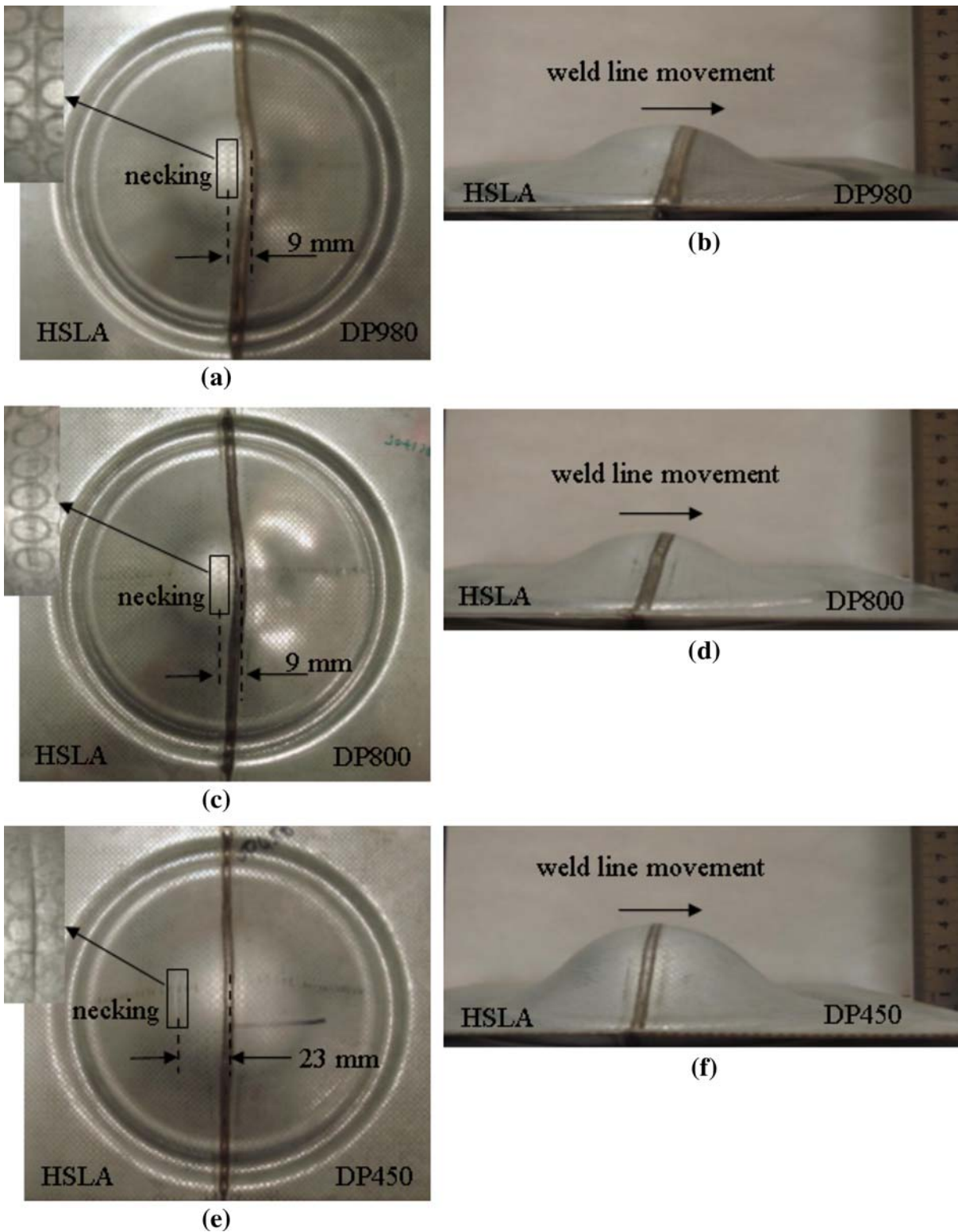
Fig. 7—Deformed dome samples of laser-welded blanks of dissimilar combinations after biaxial stretch forming.
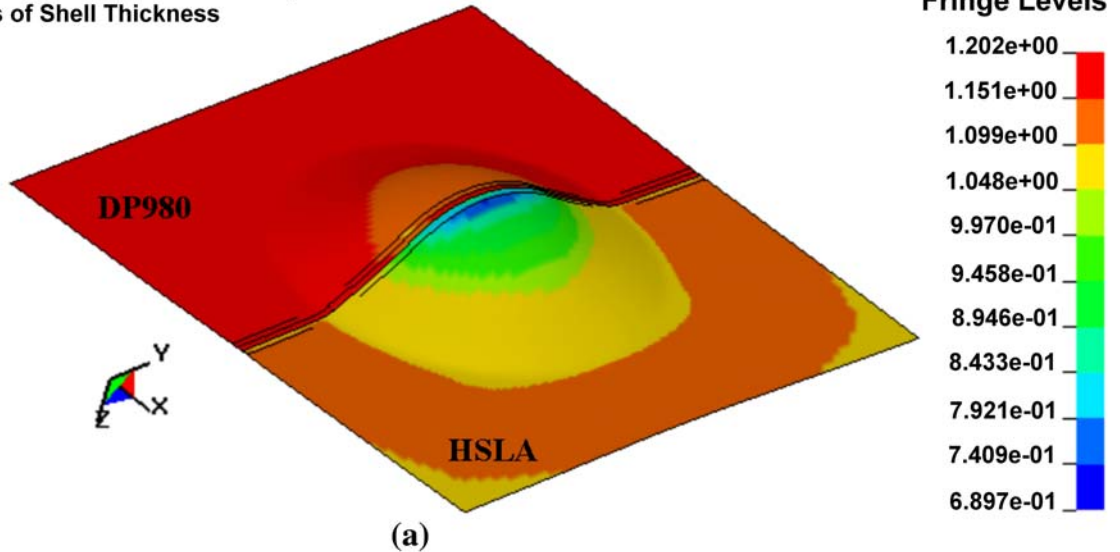
enough BM was available on each side of the hard FZ to support lateral deformation during stretch forming.

(c) Necking/fracture always takes place at the HSLA (weaker) side; hence, the forming limit properties of the weaker side, where the fracture takes, are most important.

In the present case, therefore, the HAZ and FZ properties can be neglected; this saves considerable

Time = 0.0076658, #nodes = 27724, # elem = 26791
Contours of Shell Thickness

Fringe Levels

1.202e+00
1.151e+00
1.099e+00
1.048e+00
9.970e-01
9.458e-01
8.946e-01
8.433e-01
7.921e-01
7.409e-01
6.897e-01

DP980

HSLA

(a)

TWB
Time = 0.0072328, #nodes = 10910, # elem = 10252
Contours of Shell Thickness

Fringe Levels

1.309e+00
1.247e+00
1.185e+00
1.122e+00
1.060e+00
9.979e-01
9.356e-01
8.733e-01
8.110e-01
7.488e-01
6.865e-01

DP450

HSLA

(b)
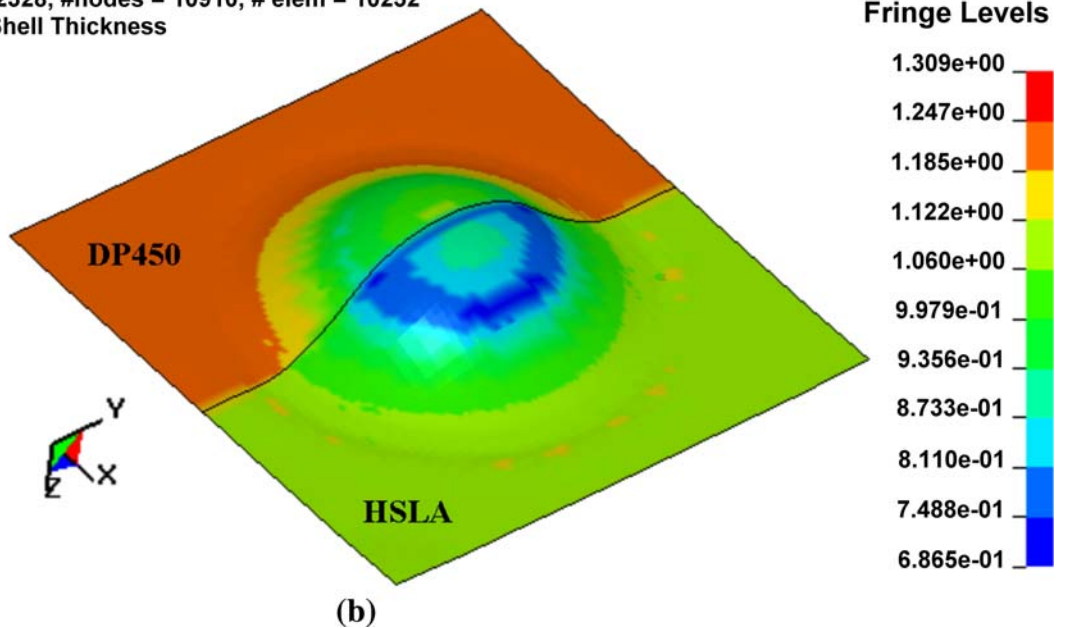
Fig. 8—Predicted thickness contours by FE simulation of (*a*) HSLA-DP980 and (*b*) HSLA-DP450.

modeling and computational time. However, if the HAZ soft zone is softer than the weaker side (BM) of the TWB, then the soft zone and properties cannot be ignored. Similarly, if the FZ is the weakest zone in the TWB or if fracture propagates across the weld, then the modeling and incorporation of the FZ properties cannot be neglected. Therefore, the microhardness profile is a good indicator in determining whether it is necessary to model the FZ and soft zone for forming simulations.

Figure 8 shows the thickness contour of the deformed surface of the HSLA-DP980 and HSLA-DP450 combination. It can be observed that necking due to maximum thinning takes place on the HSLA side in both cases, but the fracture location shifts closer to the weld line in the HSLA-DP980 blank. Similar shifts in the fracture

location were also observed during the experiments (Figure 7). The formability results can be better understood by considering the strain distribution and its effect on the weld line movement.

C. *Weld Line Movement and Strain Distribution*

The measured major and minor true strains were plotted with the distance from the pole of the hemispherical cup, to obtain the strain distribution in the deformed LDH samples. Figures 9(a) and (b) show the strain distribution profile of the HSLA-DP450 and HSLA-DP980, respectively. For comparison, the FE-predicted strain distribution is also shown. The pattern of the strain distribution profile for the HSLA-DP450 is similar to that
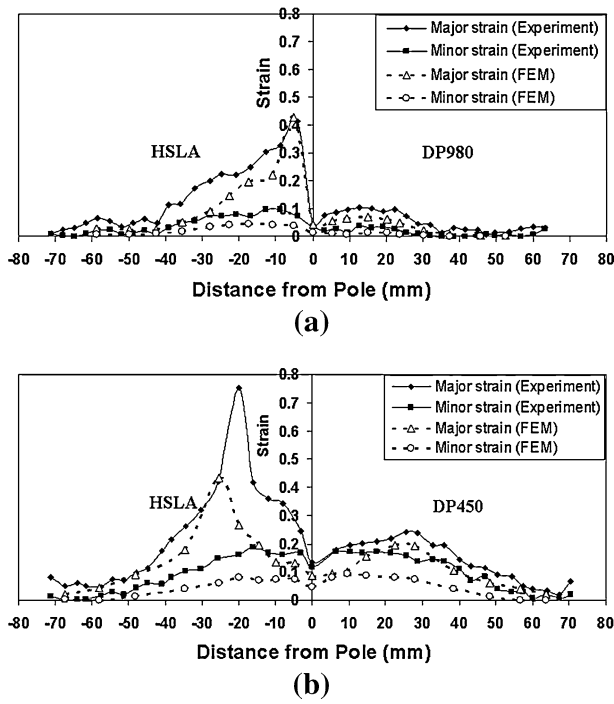
(a)

(b)

Fig. 9—Major and minor strain distribution across the weld on the dome surface of stretch-formed laser-welded blanks at necking/fracture: (*a*) HSLA-DP980 and (*b*) HSLA-DP450.

of a low-carbon monolithic steel blank. There were two clear peaks on either side of the weld, but the higher peak was on the HSLA side, away from the pole that corresponds to the failure location. The minor strains were well developed and the strain distribution on the DP450 side was more uniform. This was due to the lubrication (polyurethane sheet) at the punch-blank interface, the higher LDH, and the higher *n* value of the DP450 sheet metal. There was a minor discrepancy between the predicted and experimental peak strain. During the LDH experiment, it was difficult to stop the punch at the exact onset of diffuse necking. The experimental strain distribution corresponds to a punch depth just beyond the onset of necking, compared to the simulated strain distribution, which corresponds to the punch depth at the onset of necking. In the HSLA-DP980 combination, the peak strain at failure was on the HSLA side, close to the pole (weld line). The minor strains were not as well developed as the previous case, due to the lower LDH. In this case, the predicted strain distribution matched well with the experimental. This was likely due to the chance that the punch was stopped closer to the onset of necking. A similar strain distribution pattern was obtained for the HSLA-DP800 combination.

Figure 10 shows a comparison of the major strain distribution patterns for the HSLA-DP980 and HSLA-DP450 combinations. For the stronger side (*i.e.*, DP450 and DP980), there was more deformation in the HSLA-DP450 combination compared to the HSLA-DP980 combination. Thus, there was more nonuniform deformation and early strain localization close to the weld, when HSLA was combined with higher-strength metals such as DP980 or DP800. This was similar to the
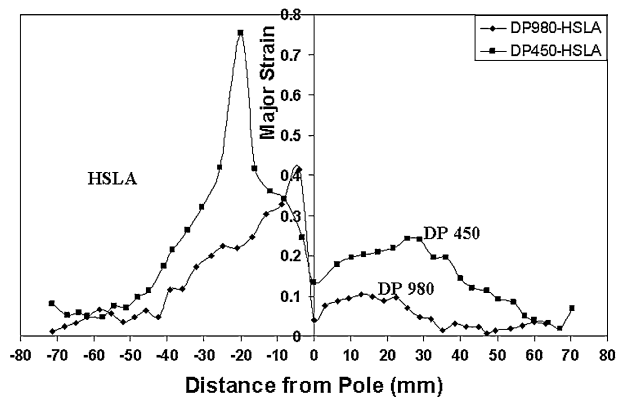

Fig. 10—Comparison of major strain distribution across the weld between HSLA-DP980 and HSLA-DP450 laser-welded combination blank at necking/fracture.
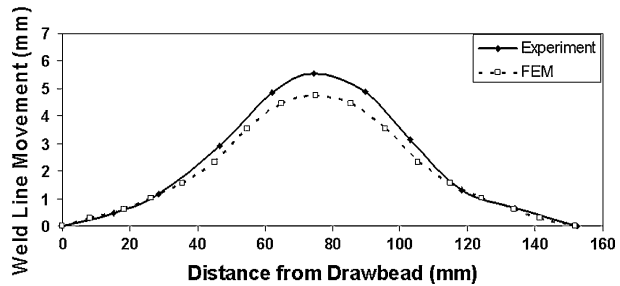

Fig. 11—Profile of weld line movement in the deformed HSLA-DP980 laser-welded blank.

results obtained in TWBs composed of materials of similar strengths and a higher thickness ratio.[8]

The weld line moved toward the stronger side during stretch forming of the dissimilar blanks (HSLA-DP450, HSLA-DP800, and HSLA-DP980). No weld line movement was observed in the HSLA-HSLA and in the other, similar combinations found in the literature.[14] A comparison of the predicted and experimental weld line movement toward the DP980 side for the HSLA-DP980 combination is shown in Figure 11. The weld line movement increased with the distance from the draw bead; it had a maximum at the pole. The pattern of weld line movement was approximately symmetric about the pole, transverse to the weld.

The weld line movement was a result of differential strain across the weld on the dome. The differential strain across the weld can be expressed well by a simple force equilibrium equation across the weld:

$$\sigma_{st} t_{st} = \sigma_{wk} t_{wk} \qquad [5]$$

hence

$$\frac{\varepsilon_{wk}^{n_{wk}}}{\varepsilon_{st}^{n_{st}}} = \frac{K_{st} t_{st}}{K_{wk} t_{wk}} = SR \ (\text{strength ratio}) \qquad [6]$$

$$\varepsilon_{st} = \left[\frac{\varepsilon_{wk}^{n_{wk}}}{SR}\right]^{\frac{1}{n_{st}}} \qquad [7]$$

where σ, ε, K, n, and t represent the flow stress, flow strain, strength coefficient, strain-hardening exponent,
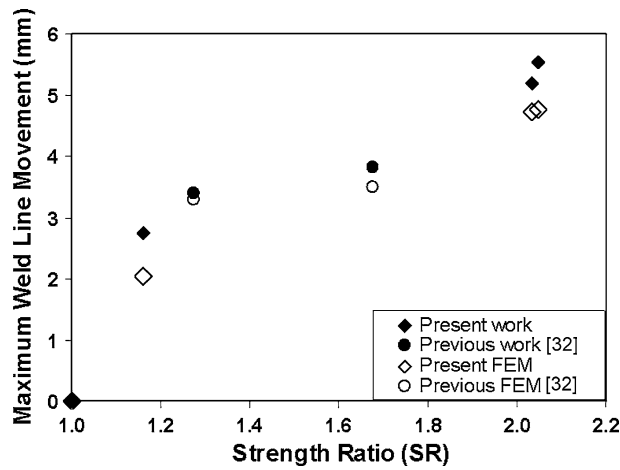
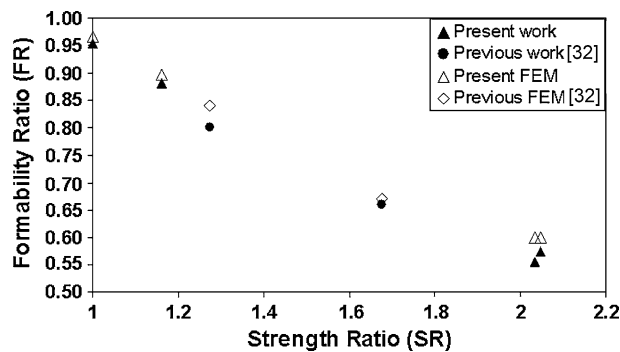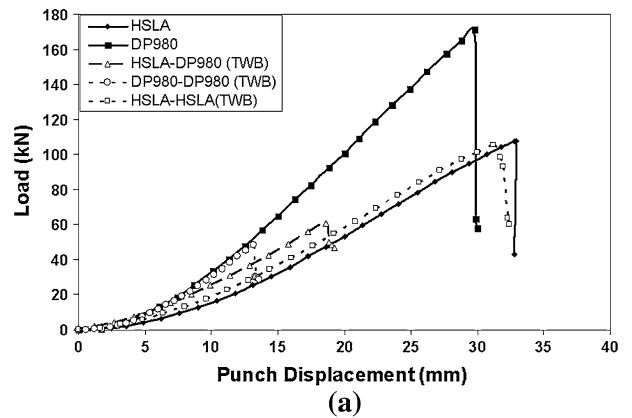Fig. 12—Effect of SR on maximum weld line movement during stretch forming of TWBs.
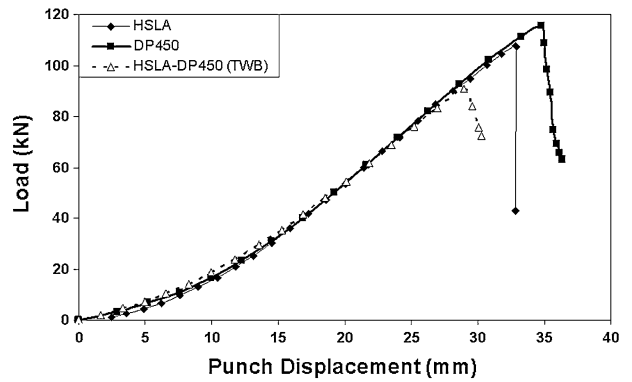

Fig. 13—Effect of SR on formability in stretch forming of TWBs.

Fig. 14—Comparison of punch-load progression curves during stretch forming for (*a*) HSLA-DP980 and (*b*) HSLA-DP450 laser-welded blank with their parent metals.

and thickness of the materials, respectively, during deformation. The subscripts "wk" and "st" are for the weaker and stronger sides, respectively, of the TWBs. Hence, the strain level on the stronger side depends on the nondimensional factor called the strength ratio (SR), as shown in Eq. [6]. Friction is neglected in the equilibrium equation, because both sides are assumed to experience the same frictional forces. Weld line movement was also observed in other laser-welded blank combinations. It was observed that the maximum weld line movement (at the pole) increases with an increase in the nondimensional parameter, SR (Figure 12). Two results from previous work[32] were also superimposed in these figures to increase the data population. As the SR increases, the strain differential between the stronger and weaker sides increases; this results in more weld line movement. It can also be observed that the formability ratio (FR) (Eq. [8]) decreases as the SR increases (Figure 13). Hence, the weld line movement resulting from the differential strain is an indication of a decrease in the TWB formability.

$$FR = \frac{\text{LDH of TWB}}{\text{LDH of parent monolithic HSLA steel sheet}} \quad [8]$$

D. Load-Displacement Curve

The load-displacement curves of the TWBs, as obtained through the data acquisition system during stretch forming, were compared to those of the parent monolithic blanks. Figure 14(a) shows a typical comparison of the load progression of the HSLA-DP980 TWB with that of the parent metal (HSLA and DP980) and laser-welded blanks of similar material (*i.e.*, HSLA-HSLA and DP980-DP980). As expected, it was found that the load that was required to deform the DP980 steel was higher than that required for the HSLA steel, because of its significantly higher flow strength. The punch load for the TWBs of the dissimilar-material combination (HSLA-DP980) was in between the punch load of the parent monolithic sheets at any given punch displacement. The peak load that was required to deform the TWB, however, was less as compared to both the parent sheets. This was due to the lower LDH of the TWBs and the smaller punch-contact area at the instance of fracture. There was a significant difference in the punch-load progression between the similar laser-welded blank (HSLA-HSLA and DP980-DP980) combination. The maximum punch load for the DP980-DP980 combination was much lower as compared to the HSLA-HSLA combination and monolithic DP980. This was due to the strain localization and early
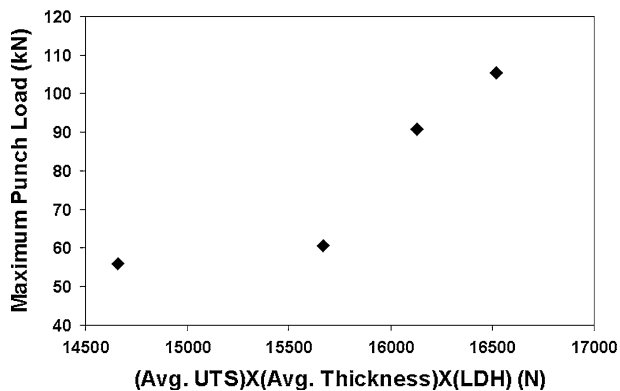
Fig. 15—Effect of UTS, thickness, and LDH on punch load of TWBs.

fracture in the soft zone at the outer HAZ, resulting in the lower LDH of the DP980-DP980 combination.[22] Figure 14(b) shows a comparison of the load progression between the HSLA-DP450 TWB with the parent metals (HSLA and DP450). It was found that, at any punch displacement, the punch load was similar in all of the cases. This was due to the small differences between the flow strength of the base materials (HSLA and DP450) (Figure 2). However, the maximum punch load of the TWB was less compared to both of the parent metals. This was due to the lower LDH of the laser-welded blank compared to both the parent metals. Figure 15 shows that the maximum load during the stretch forming of the TWB depends on the average UTS and the average thickness of both the parent metal and the LDH of the laser-welded blanks.

VI. CONCLUSIONS

In this study, the formability of welded blanks that are made up of two different materials has been evaluated and compared to monolithic blanks of the parent materials and to welded blanks made up of only one material. The formability has been measured using the Hecker's LDH test; the results have been correlated using an FE analysis to validate the model as a useful tool for predicting formability of TWBs. The effects of property changes in the weld region, such as the HAZ softening and FZ hardening, were evaluated by their impact on the TWB formability and strain distribution. The conclusions of this study are the following.

1. The formability of TWBs made up of two different materials was less than the formability of each of the parent metals. When softening was observed in the HAZ of the higher-strength materials, such as the DP980 and DP800, the strain and fracture were localized in the softened zone in single-material welded blanks; however, when these materials were combined with the lower-strength HSLA, strain and failure were localized in the HSLA side of the TWB. This was due to the higher strength and hardness of the soft zone as compared to that of

the HSLA BM, which caused strain localization to shift from the soft zone to the HSLA side.

2. Calculations both with and without the incorporation of soft zone and FZ properties in the FE simulations showed similar LDH results (less than 0.1 pct difference in the LDH), for dissimilar-material combination blanks. During FE modeling, therefore, the soft zone and FZ can be omitted. This has the potential to save set-up and computational time in formability analysis, because the soft zone and fusion hard zone properties do not need to be measured or modeled. However, if the soft zone will be softer than the weaker side of a dissimilar combination, then the modeling of the soft zone will be required and cannot be neglected.

3. The LDH, maximum weld line movement, and fracture location during stretch forming of a TWB depend on a nondimensional parameter, SR. Increased SR, decreased formability, and increased weld line movement resulted in nonuniform strain distributions.

4. The punch-load progression for the TWBs depends on the thickness and strength of both the parent metal and the LDH achieved during stretch forming.

REFERENCES

1. *Advanced High Strength Steel Application Guidelines*, version 4, World Auto Steel, March 2009, www.worldautosteel.org.
2. Auto/Steel Partnership: *Tailor Welded Blank Design and Manufacturing Manual*, Technical Report, 1995.
3. B. Kinsey, Z. Liu, and J. Cao: *J. Mater. Process. Technol.*, 2000, vol. 99, pp. 145–53.
4. C.H. Cheng, M. Jie, C.L. Chan, and C.L. Chow: *Int. J. Mech. Sci.*, 2007, vol. 49, pp. 217–29.
5. N. Sreenivasan, M. Xia, S. Lawson, and Y. Zhou: *J. Eng. Mater. Technol. (Trans. ASME)*, 2008, vol. 130 (4), 041004.
6. M. Xia, N. Sreenivasan, S. Lawson, and Y. Zhou: *J. Eng. Mater Technol. (Trans. ASME)*, 2007, vol. 129, pp. 446–52.
7. S.K. Panda, N. Sreenivasan, M. Kuntz, and Y. Zhou: *J. Eng. Mater. Technol. (Trans. ASME)*, 2008, vol. 130 (4), 041003.
8. S.K. Panda, D. Ravi Kumar, H. Kumar, and A.K. Nath: *J. Mater. Process. Technol.*, 2007, vol. 183, pp. 321–32.
9. D. Dry, W. Wadell, and D.R.J. Owen: *Sci. Technol. Weld. Join.*, 2002, vol. 7 (1), pp. 11–18.
10. G. Kridli, P.A. Friedman, and A.M. Sherman: SAE Technical Paper No. 2000-01-0772, SAE, Detroit, Michigan, March 6–9, 2000, pp. 1–9.
11. L.C. Chan, S.M. Chan, C.H. Cheng, and T.C. Lee: *J. Eng. Mater. Technol.*, 2005, vol. 127, pp. 179–85.
12. Y. Choi, Y. Heo, H.Y. Kim, and D. Seo: *J. Mater. Process Technol.*, 2000, vol. 108, pp. 1–7.
13. Y. Heo, Y. Choi, H. Kim, and D. Seo: *J. Mater. Process. Technol.*, 2001, vol. 111, pp. 164–69.
14. S.K. Panda and D. Ravi Kumar: *J. Mater. Process. Technol.*, 2008, vol. 204, pp. 70–79.

15. S. Gaied, J. Roelandt, F. Pinard, F. Schmit, and M. Balabane: *J. Mater. Process. Technol.*, 2009, vol. 209, pp. 387–95.
16. H. Shao, J. Gould, and C. Albright: *Metall. Mater. Trans. B*, 2007, vol. 38B, pp. 321–31.
17. S.S. Hecker: *Met. Eng. Q.*, 1974, pp. 30–36.
18. K. Narasimhan and V.M. Nadedkar: *Trans. Ind. Inst. Met.*, 1996, vol. 49, pp. 659–76.
19. N. Yurioka, H. Suzuki, S. Ohshita, and S. Saito: *Weld. J.*, 1980, vol. 62, pp. 147s–153s.
20. F.M. Al-Abbasi and J.A. Nemes: *Int. J. Solid. Struct.*, 2003, vol. 40, pp. 3379–91.
21. D.V. Wilson: *Metall. Technol.*, 1980, vol. 7, pp. 282–92.
22. S.K. Panda, M.L. Kuntz, and Y. Zhou: *Sci. Technol. Weld. Join.*, 2009, vol. 14, pp. 52–61.
23. R.W. Davies, G.J. Grant, M.A. Khaleel, M.T. Smith, and H. Eddie Oliver: *Metall. Mater. Trans. A*, 2001, vol. 32A, pp. 275–83.
24. J.O. Hallquist: *LS-DYNA Keyword User's Manual, Version 970*, 2003, http://www.lstc.com/ (Registered trademark of Livermore Software Technology Corporation, Livermore, CA).
25. W. Bleck, Z. Deng, K. Papamantellos, and C.O. Gusek: *J. Mater. Process. Technol.*, 1998, vol. 83, pp. 223–30.
26. T. Belytschko, J.I. Lin, and C. Tsay: *Comput. Methods Appl. Mech. Eng.*, 1984, vol. 42, pp. 225–51.
27. A.K. Ghosh: *Int. J. Mech. Sci.*, 1977, vol. 19, pp. 457–70.
28. F. Barlat and J.I. Lian: *Int. J. Plast.*, 1989, vol. 5, pp. 51–56.
29. M. Xia, E. Biro, Z. Tian, and Y. Zhou: *ISIJ Int.*, 2008, vol. 48, pp. 809–14.
30. V.H. Baltazar Hernandez, M.L. Kuntz, M.I. Khan, and Y. Zhou: *Sci. Technol. Weld. Join.*, 2008, vol. 13, pp. 769–76.
31. N. Sreenivasan, M. Kuntz, and Y Zhou: *Int. Conf. Mater. Sci. Technol. (MS&T) Automotive*, Detroit, MI, 2007, pp. 267–80.
32. S.K. Panda: Doctoral Thesis, Indian Institute of Technology, Delhi, India, 2007, chap. 6, pp. 112–61.